Improving the Performance of Lithium Manganese Phosphate Through Divalent Cation Substitution

Guoying Chen[*, z] and Thomas J. Richardson[*]

Environmental Energy Technologies Division

Lawrence Berkeley National Laboratory

Berkeley, California 94720 USA

Abstract

Highly crystalline samples of $LiMnPO_4$ and its analogs with partial substitution of Mn by divalent Mg, Cu, Zn, and Ni were prepared by hydrothermal synthesis and characterized by x-ray diffraction and infrared spectroscopy. Chemical oxidation produced two-phase mixtures of the initial phases $LiMn_{(1-y)}M_yPO_4$ and the delithiated forms, $Li_yMn_{(1-y)}M_yPO_4$, all with the olivine structure. The extent of oxidation depended upon the quantity of oxidizing agent used and on the identity of the substituent ions. Mg, Ni and Cu were found to increase the level of delithation relative to that in pure $LiMnPO_4$. Mg was also shown to reduce the tendency of the oxidized phase to absorb water.

---

[*] Electrochemical Society Active Member

[z] E-mail: gchen@lbl.gov

Introduction

Olivine-type $LiMPO_4$ (M = Fe, Mn, Co, Ni) compounds have an orthorhombic comprised of close-packed phosphate anions with M^{2+} ions in corner-sharing MO_6 sites and Li ions in edge-sharing LiO_6 sites.[1] The strong P-O covalent bond gives these materials good stability and makes them attractive as positive electrodes for lithium batteries in vehicle applications. $LiMnPO_4$ (lithiophilite) cycles at a nearly constant potential of 4.1 V vs. Li/Li^+, which is well-suited to use in standard battery configurations. In contrast with $LiFePO_4$, however, the manganese compound suffers from poor Li extraction and insertion kinetics. Many factors have been considered to contribute to the slow phase transition, including the electronic and ionic conductivities, the Jahn-Teller effect in Mn^{3+}, interface strain due to the large volume change between $LiMnPO_4$ and $MnPO_4$, and the metastable nature of the delithiated phase.[2-4] Although the mechanism of the two-phase reaction has not been identified, it is likely that it is similar to that of the $LiFePO_4/FePO_4$ system.[5] Previous efforts[6-9] to improve the performance of stoichiometric $LiMnPO_4$ have mostly been limited to particle size minimization, which increases the rate and utilization, but inevitably decreases the volumetric energy density of the electrode.

Studies have shown that M-site doping with divalent cations such as Mg^{2+}, Zn^{2+}, Cu^{2+}, Ni^{2+} and Co^{2+} can improve the performance of $LiFePO_4$.[10-14] Yamada has intensively investigated the $Li(Mn,Fe)PO_4$ solid solution system[1,15-18], and found that although Fe-substituted $LiMnPO_4$ has kinetics and utilization properties superior to those of pure $LiMnPO_4$, for Mn content above 80 %, Fe does not provide sufficient stabilization, and some decomposition takes place on extraction of lithium. Solid-state

synthesis of $LiMnPO_4$ and $LiMn_{(1-y)}M_yPO_4$ (M = Mg, Ca, Zn, Ni, Co, Cu, Al, B, Cr and Nb) samples at high temperatures has been reported in patents by Valence Technology Inc.,[19-20] Phase-pure, well-formed $LiMnPO_4$ crystals have recently been synthesized by low-temperature hydrothermal methods.[21-23] Chen et al.[22-23] prepared $LiMn_{(1-y)}Mg_yPO_4$ crystals with a wide range of Mg substitution. Here we report hydrothermal syntheses of M^{2+}-substituted $LiMnPO_4$ crystals with M = Ni, Cu and Zn. The reactivities of these samples and one Mg-substituted sample were examined through chemical oxidation, and a mechanism is proposed to describe the effects of substitution. Electrochemical properties of the synthesized phosphates will be reported in a future publication.

Experimental

$LiMnPO_4$ crystals were synthesized using the hydrothermal method described previously for $LiFePO_4$.[5] Equimolar amounts of $MnSO_4.H_2O$ (Mallinckrodt, Inc) and H_3PO_4 (85%, J. T. Baker) were mixed in 30 ml deionized and deoxygenated water to give an Mn concentration of 1.0 M. A 1.5 M LiOH (Spectrum) solution was added slowly with stirring to give Mn:P:Li equal to 1:1:3 and a final pH of 10. Substantial precipitation occurred during this step. After stirring under helium for another 5 min, the reaction mixture was transferred to a 125 ml Teflon-lined reactor, which was tightly sealed after purging with helium, then held at 220 °C for 5 h. On cooling to room temperature, the off-white precipitate was filtered, thoroughly washed with deionized water, and dried in a vacuum oven at 60 °C for 24 h. The substituted $LiMnPO_4$ samples were prepared using the same procedure, except that a 9:1 molar mixture of $MnSO_4.H_2O$ with $Mg(NO_3)_2.6H_2O$ (>99%, EM Science), Ni $SO_4.6H_2O$ (Johnson Matthey Electronics),

$CuSO_4.5H_2O$ (99%, J. T. Baker) or $ZnSO_4.7H_2O$ (99%, Aldrich), was dissolved before adding the H_3PO_4 and LiOH solutions. Delithiation was achieved by stirring the samples in aliquots of a 0.1 M solution of nitronium tetrafluoroborate (NO_2BF_4, 95+%, Aldrich) in acetonitrile for 24 h at room temperature in an argon-filled glovebox with $O_2 < 1$ ppm and $H_2O < 2$ ppm.

X-ray diffraction (XRD) patterns were acquired using a Panalytical Xpert Pro diffractometer equipped with monochromatized Cu Kα radiation. The scan rate was 0.0025°/s from 10° to 70° 2θ in 0.01° steps. Lattice parameters and phase ratios in the oxidized samples were determined by pattern refinement using Riqas software (Materials Data, Inc.). Scanning electron microscopy (SEM) images were obtained using a Hitachi S-4300 SE/N microscope at 20 and 10 kV accelerating voltages, with energy dispersive X-ray analysis (EDX) and elemental mapping using the Noran System SIX. Fourier transform infrared spectroscopy (FTIR) measurements were performed on KBr pellets using a Nicolet 6700 spectrometer in transmission mode with a spectral resolution of 4 cm^{-1}.

Results and Discussion

Synthesis and Characterization

XRD patterns of substituted and unsubstituted $LiMnPO_4$ samples are shown in Fig. 1. The unsubstituted and Mg-substituted samples were phase pure, while small amounts of unidentified impurities were detected in Ni-, Cu- and Zn-substituted samples. This is probably due to lower solubility of the Ni, Cu or Zn precursor in the reaction mixture, resulting in formation of the substituted olivine before complete uptake was

possible, rather than a true limit of solubility in the parent compound. Lattice parameters obtained from Rietveld refinement of the whole patterns are listed in Table 1. The unsubstituted $LiMnPO_4$ had a = 10.4474 Å, b = 6.1016 Å, c = 4.7506 Å and V = 302.83 $Å^3$, in good agreement with the reported values.[24] M^{2+} substitution decreased all three lattice parameters. The cell volume decreased 0.8% for Mg^{2+}, 0.6% for Ni^{2+}, 0.3% for Cu^{2+} and 0.4% for Zn^{2+} substitution, consistent with their smaller ionic radii. The lattice parameters of our $LiMg_{0.1}Mn_{0.9}PO_4$ sample were slightly smaller than those reported by Chen et al., whose crystals were much larger and needle-like.[23] Site occupancy refinement showed no excess electron density on the lithium site in each case. The Scherrer crystallite sizes were about 30 nm for all samples except the Mg-substituted one, which was 48 nm.

SEM images of the hydrothermal synthesized samples are shown in Fig. 2. The unsubstituted $LiMnPO_4$, Ni-, Cu- and Zn-substituted samples were elongated diamond-shaped aggregates composed of small crystals about 200 nm in size. The morphology of the Mg-substituted sample was quite different. It consisted of smooth, hexagonal-shaped crystal plates measuring about 0.8 μm x 0.4 μm x 0.1 μm. EDX and elemental mapping (Fig. 3) showed a uniform distribution of Mn, Mg, P and O. The atomic ratio of Mn to Mg was 8.8:1, consistent with the intended ratio of 9:1, and was constant among crystals and at different locations on individual crystals.

Chemical delithiation

To investigate the effects of substitution on reactivity, the extent of lithium extraction by the NO_2BF_4 solution was determined by XRD. In each case, the oxidized

samples contained of a second olivine-type phase along with unreacted starting material. The potential of the NO_2^+/NO_2 couple is *ca.* 5.1 V *vs.* Li/Li^+, more than sufficient to remove Li from $LiMnPO_4$ according to:

$$LiMnPO_4 + xNO_2BF_4 \rightarrow (1\text{-}x)LiMnPO_4 + xMnPO_4 + xLiBF_4 + xNO_2 \qquad [1]$$

In the case of a 10 % substituted olivine in which the substituent, M, is not oxidized, we may expect the reaction to proceed as follows:

$$LiM_{0.1}Mn_{0.9}PO_4 + 0.9xNO_2BF_4 \rightarrow (1\text{-}x)LiM_{0.1}Mn_{0.9}PO_4 + xLi_{0.1}M_{0.1}Mn_{0.9}PO_4 + 0.9xLiBF_4 + 0.9xNO_2 \qquad [2]$$

XRD patterns of samples treated with an amount of NO_2BF_4 sufficient to extract 50 % of the active lithium are shown in Fig. 4. The lattice parameters of the delithiated phases are given in Table 1. Ten percent of the unsubstituted $LiMnPO_4$ had been converted to the oxidized phase after 24 h. Under the same conditions, the Zn^{2+}-substituted, Cu^{2+}-substituted and Ni^{2+}-substituted samples were 2 %, 14% and 18% oxidized, respectively. The Mg^{2+}-substituted sample was the most reactive, with 23% of the delithiated phase formed. Thus, Mg^{2+}, Ni^{2+} and Cu^{2+} substitution were beneficial, while Zn^{2+} had a negative effect.

The Mg^{2+}-substituted crystals were several times larger than those of the other phosphates, which were aggregated crystals about 200 nm size. The observed improvement is clearly not due to a size effect, but rather to the presence of Mg^{2+} in the

structure. At this point it is unclear why the Zn^{2+}-substituted sample was so difficult to delithiate. One possibility is the presence of an insoluble impurity on the surface that hinders the reaction. Synthesis experiments carried out using different metal precursors, solution concentrations and/or pH may provide the answer.

FTIR absorption spectra of the unsubstituted and substituted samples are compared in Fig. 5a. The bands at frequencies > 900 cm^{-1} are attributed to the symmetric and antisymmetric stretching vibration of $PO4^{3-}$ anion, while those at lower frequencies include bending vibrations of the anion and lattice modes.[25] The low frequency bands were largely unaffected by substitution. The higher frequency bands, however, were shifted toward higher energy, suggesting an increase in P-O bond strength in the substituted samples. The FTIR spectra of the partially oxidized samples are shown in Fig. 5b. In each case, a new band appeared at about 1075 cm^{-1}, increasing in intensity with the amount of the oxidized phase present.

When unsubstituted samples were treated with increasing quantities of the NO_2BF_4 solution, the extent of delithiation increased, reaching 30 % and 70 % for NO_2BF_4:$LiMnPO_4$ ratios of 1:1 and 2:1 respectively after 24 h reaction (Fig. 6a). The result is consistent with the report by Yamada et al[16] where 70% of delithiation was achieved after reaction for 48 hr at a ratio of 2:1. In contrast, oxidation of Mg-substituted samples reached 60 % and 100 % under the same conditions (Fig. 6b). The domain sizes of the delithiated phases increased monotonically with the extent of delithiation in each case, to a maximum of 10 nm for unsubstituted $LiMnPO_4$, and to 18 nm for the fully oxidized Mg-substituted sample.

It has been reported[1-2] that partially and fully delithiated $LiMnPO_4$ samples absorb water in air. We indentified the hydration products by XRD as $MnPO_4 \cdot 1.5H_2O$ and $Mn_{0.9}Mg_{0.1}PO_4.1.5H_2O$. This instability, attributed to the elastic energy accumulated inside the Jahn-Teller deformed lattice, complicates the isolation and characterization of the pure $MnPO_4$.[3] $Li_{0.1}Mg_{0.1}Mn_{0.9}PO_4$ was found to be stable in air when coexisting with $LiMg_{0.1}Mn_{0.9}PO_4$, slowly converting to $Li_{0.1}Mg_{0.1}Mn_{0.9}PO_4.1.5H_2O$ only in fully oxidized samples. Our crystal samples of both $Li_{0.1}Mg_{0.1}Mn_{0.9}PO_4$ and $MnPO_4$ were stable when kept in an inert atmosphere.

Possible mechanism of the substituent effect

The ionic radius of Mn^{2+} in octahedral coordination is 0.98 Å,[26] which decreases to 0.785 Å upon oxidation to Mn^{3+}. The substituent ion radii are 0.83 Å for Ni^{2+}, 0.86 Å for Mg^{2+}, 0.87 Å for Cu^{2+} and 0.88 Å for Zn^{2+}, and they remain the same in the lithiated and delithiated phases. Assuming that the phase transformation progresses through the "reactive transition zone" mechanism as described in $LiFePO_4$, [5] Mn-site substitution may influence $LiMnPO_4$ oxidation in several ways. The presence of the larger ions, which are more compatible with the olivine structure, may stabilize the lattice against the strain created by the small Jahn-Teller Mn^{3+} ions. The decreased reactivity of $Li_{0.1}Mg_{0.1}Mn_{0.9}PO_4$ in air, as well as the presence of larger crystalline domains in the Mg-substituted material point toward such stabilization. This may, in turn, create a more favorable boundary between the two phases and facilitate the conversion of one phase to the other without loss of coherence.

Substitution also decreases the volume change between the two end members (Fig. 7), in part because M^{2+} is smaller than Mn^{2+} but larger than Mn^{3+}, and also because the Li associated with the electrochemically inactive M^{2+} remains in the substituted delithiated phase. For the unsubstituted sample, the volume change between $LiMnPO_4$ and $MnPO_4$ is 9.5%, while the changes are 8.2% for Zn substitution, 8.0% for Cu, 7.9% for Ni and 7.8% for Mg. The mismatch in the *ac* plane, in which the phase boundary is probably located, is also reduced, with the largest decrease observed for Mg.

Finally, if the products of decomposition of the delithiated phases contains only Mn^{3+}, a substantial de-mixing of ions is required, presenting a kinetic barrier to rearrangement.

Conclusions

Divalent cation-substituted $LiMnPO_4$ crystals were synthesized by a hydrothermal method and characterized by XRD and FTIR. The substituents resided only on Mn sites. Chemical delithiation produced two-phase mixtures of lithiated and delithiated olivine-type phases. The presence of Mg^{2+}, Ni^{2+} and Cu^{2+} resulted in increased conversion to the delithiated phases. Further, Mg-substitution improved the stability of the delithiated phase with respect to hydration in air. These effects are attributed to stabilization of the oxidized phases due to the ion sizes and the incomplete removal of lithium from the lattice.

Acknowledgements

This work was supported by the Assistant Secretary for Energy Efficiency and Renewable Energy, Office of FreedomCAR and Vehicle Technologies of the U. S. Department of Energy under Contract No. DE-AC02-05CH11231.

Table 1. Cell parameters of substituted and unsubstituted $LiMnPO_4$

		a (Å)	b (Å)	c (Å)	V (Å^3)
$LiMnPO_4$	Fresh	10.4474	6.1016	4.7506	302.83
	Delithiated	9.6660	5.9390	4.7785	274.10
Mg-$LiMnPO_4$	Fresh	10.4189	6.0842	4.7408	300.52
	Delithiated	9.7045	5.9672	4.7820	276.92
Ni-$LiMnPO_4$	Fresh	10.4197	6.0768	4.7527	300.93
	Delithiated	9.7221	5.9613	4.7781	276.92
Cu-$LiMnPO_4$	Fresh	10.4181	6.1031	4.7466	301.80
	Delithiated	9.7344	5.9829	4.7688	277.62
Zn-$LiMnPO_4$	Fresh	10.434	6.0893	4.7447	301.46
	Delithiated	9.6237	5.9911	4.7986	276.67

References

[1] A. Yamada, Y. Takei, H. Koizumi, N. Sonoyama, R. Kanno, K. Itoh, M. Yonemura and T. Kamiyama, *Chem. Mater.*, **18**, 804 (2006).

[2] C. Delacourt, L. Laffont, R. Bouchet, C. Wurm, J.-B. Leriche, M. Morcrette, J.-M. Tarascon, and C. Masquelier, *J. Electrochem. Soc.*, **152**, A913 (2005).

[3] A. Yamada and S.-C. Chung, *J. Electrochem. Soc.*, **148**, A960 (2001).

[4] M. Yonemura, A. Yamada, Y. Takei, N. Sonoyama, and R. Kanno, *J. Electrochem. Soc.*, **151**, A1352 (2004).

[5] G. Chen, X. Song, and T. J. Richardson, *Electrochem. Solid-State Lett.*, **9**, A295 (2006).

[6] C. Delacourt, P. Poizot, M. Morcrette, J.-M. Tarascon, and C. Masquelier, *Chem. Mater.*, **16**, 93 (2004).

[7] N.-H. Kwon, T. Drezen, I. Exnar, I. Teerlinck, M. Isono and M. Graetzel, *Electrochem. Solid-State Lett.*, **9**, A277 (2006).

[8] T. R. Kim, D. H. Kim, H. W. Ryu, J. H. Moon, J. H. Lee, S. Boo and J. Kim, *J. Phys. and Chem. Solids*, **68**, 1203 (2007).

[9] T. Drezen, N.-H. Kwon, P. Bowen, I. Teerlinck, M. Isono and I. Exnar, *J. Power Sources*, **174**, 949 (2007).

[10] D. Wang, H. Li, S. Shi, X. Huang and L. Chen, *Electrochem. Acta.*, **50**, 2955 (2005).

[11] G. X. Wang, S. L. Bewlay, K. Konstantinov, H. K. Liu, S. X. Dou and J.-H. Ahn, *Electrochem. Acta.*, **50**, 443 (2004).

[12] T.-H. Teng, M.-R. Yang, S.-H. Wu and Y.-P. Chiang, *Solid State Commun.*, **142**, 389 (2007).

[13] H. Liu, Z. Cao, L. J. Fu, C. Li, Y. P. Wu and H. Q. Wu, *Electrochem. Commun.*, **8**, 1553 (2006).

[14] J. F. Ni, H. H. Zhou, J. T. Chen and X. X. Zhang, *Mater. Lett.*, **59**, 2361 (2005).

[15] A. Yamada, Y. Kudo and K.-Y. Liu, *J. Electrochem. Soc.*, **148**, A747 (2001).

[16] A. Yamada and S.-C. Chung, *J. Electrochem. Soc.*, **148**, A960 (2001).

[17] A. Yamada, Y. Kudo and K.-Y. Liu, *J. Electrochem. Soc.*, **148**, A1153 (2001).

[18] A. Yamada, M. Hosoya, S.-C. Chung, Y. Kudo, K. Hinokuma, K.-Y. Liu and Y. Nishi, *J. Power Sources*, **119-121**, 232 (2003).

[19] J. Barker, M. Y. Saidi and T. E. Kelley, US Patent 7,041,239, 2006 (Valence Technology, Inc.).

[20] M. Y. Saidi and H. Huang, US Patent 7,060,238, 2006 (Valence Technology, Inc.).

[21] H. Fang, L. Li and G. Li, *Chem. Lett.*, **36**, 436 (2007).

[22] J. Chen, S. Wang and M. S. Whittingham, *J. Power Sources*, **174**, 442 (2007).

[23] J. Chen, M. J. Vacchio, S. Wang, N. Chernova, P. Y. Zavalij, M. S. Whittingham, *Solid State Ionics*, **178**, 1676 (2008).

[24] S. Geller and J. L. Durand, *Acta Cryst.*, **13**, 325 (1960).

[25] C. M. Burba and R. Frech, *J. Electrochem. Soc.*, **151**, A1032 (2004).

[26] R. D. Shannon, *Acta Cryst.*, **A32**, 751 (1976).

Figure captions

1. X-ray diffraction patterns of hydrothermal synthesized samples: a) $LiMnPO_4$, b) Mg-substituted $LiMnPO_4$, c) Ni-substituted $LiMnPO_4$ d) Cu-substituted $LiMnPO_4$, and e) Zn-substituted $LiMnPO_4$. * indicates unidentified impurity peaks • indicates Al peaks from sample holder.
2. SEM images of hydrothermal synthesized samples: a) $LiMnPO_4$, b) Mg-substituted $LiMnPO_4$, c) Ni-substituted $LiMnPO_4$ d) Cu-substituted $LiMnPO_4$, and e) Zn-substituted $LiMnPO_4$.
3. SEM image and the corresponding element maps of Mg-substituted $LiMnPO_4$
4. XRD patterns of the oxidized samples prepared using a 1:2 ratio of NO_2BF_4 to the indicated phosphates: a) $LiMnPO_4$, b) Mg-substituted $LiMnPO_4$, c) Ni-substituted $LiMnPO_4$ d) Cu-substituted $LiMnPO_4$, and e) Zn-substituted $LiMnPO_4$.
5. FTIR absorption spectra of a) hydrothermally synthesized samples and b) samples oxidized using a 1:2 ratio of NO_2BF_4 to the phosphates.
6. XRD patterns of samples oxidized using indicated NO_2BF_4 to phosphate ratios: a) $LiMnPO_4$ and b) Mg-substituted $LiMnPO_4$; c) oxidation percentage comparison.

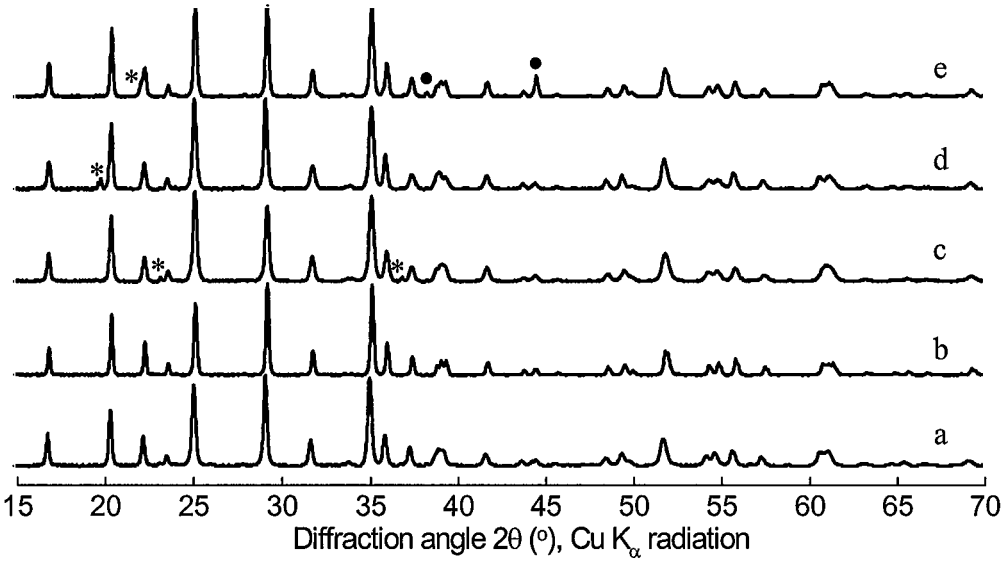

Chen and Richardson, Figure 1

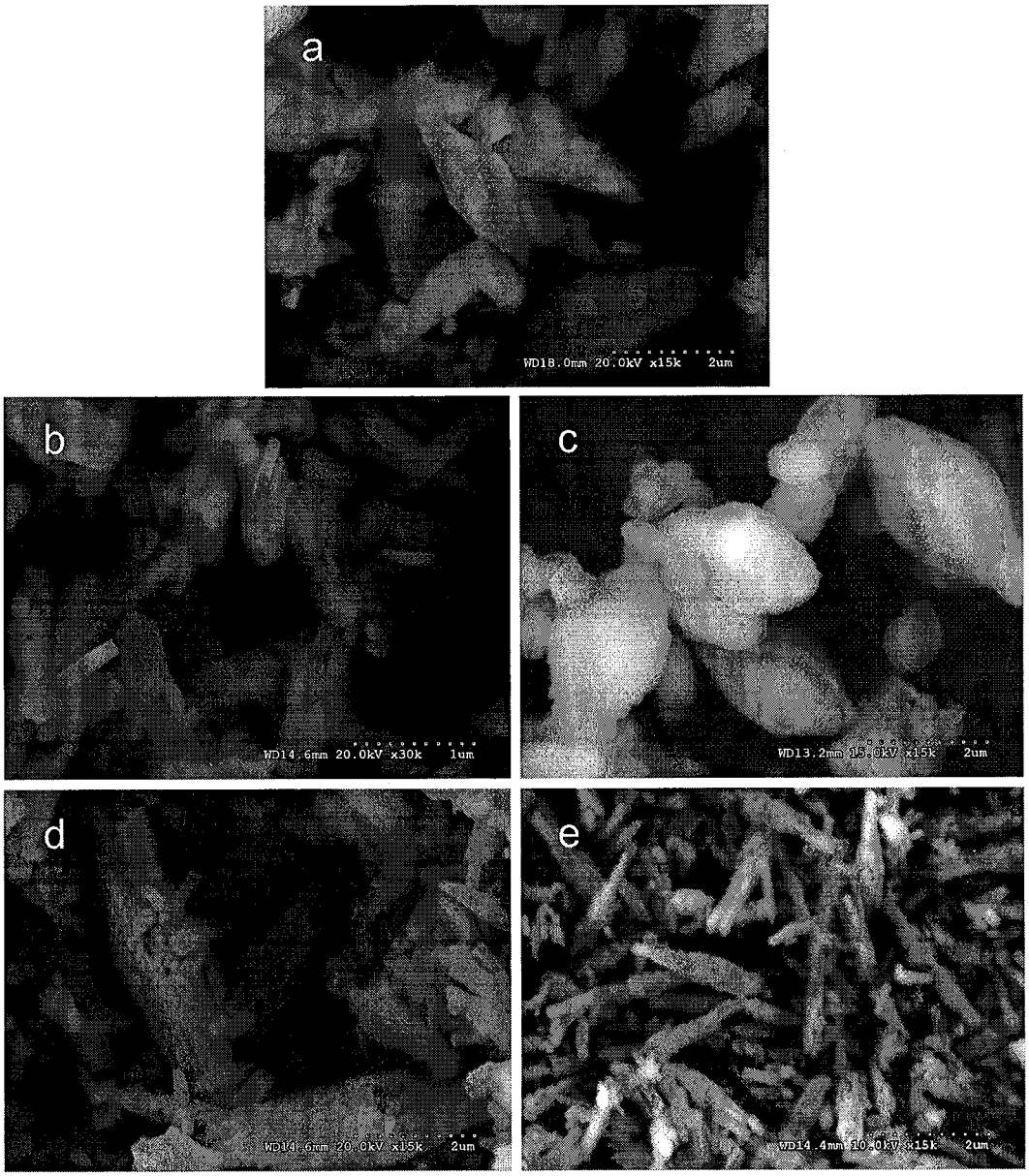

Chen and Richardson, Figure 2

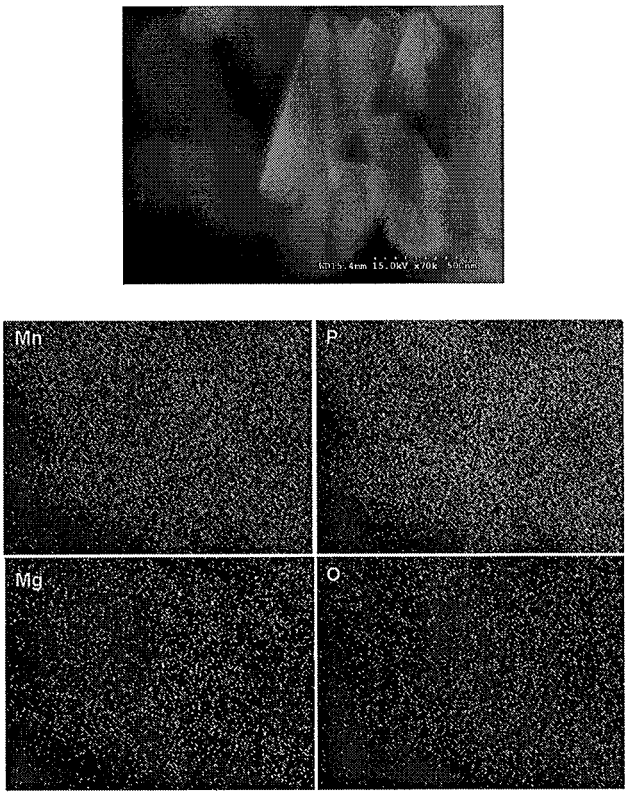

Chen and Richardson, Figure 3

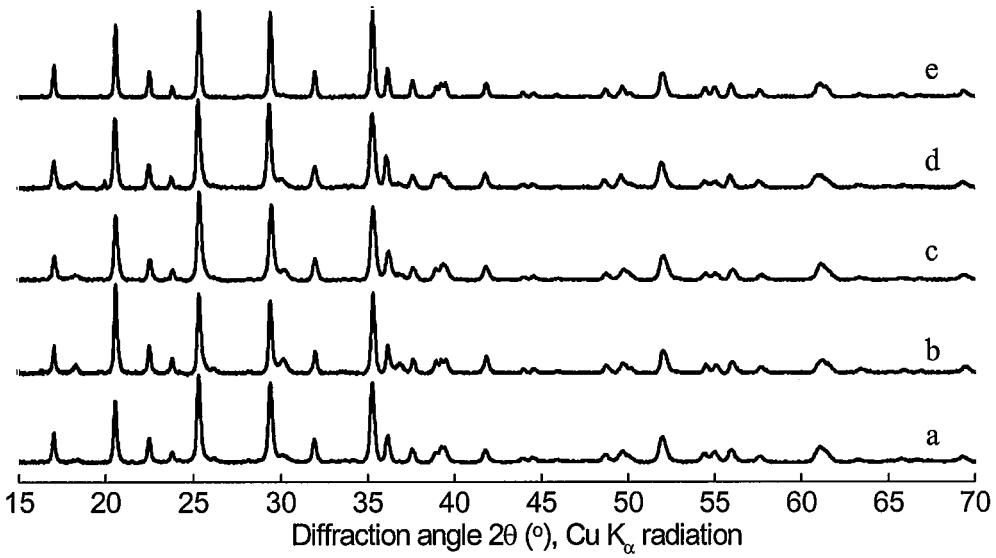

Chen and Richardson, Figure 4

a)

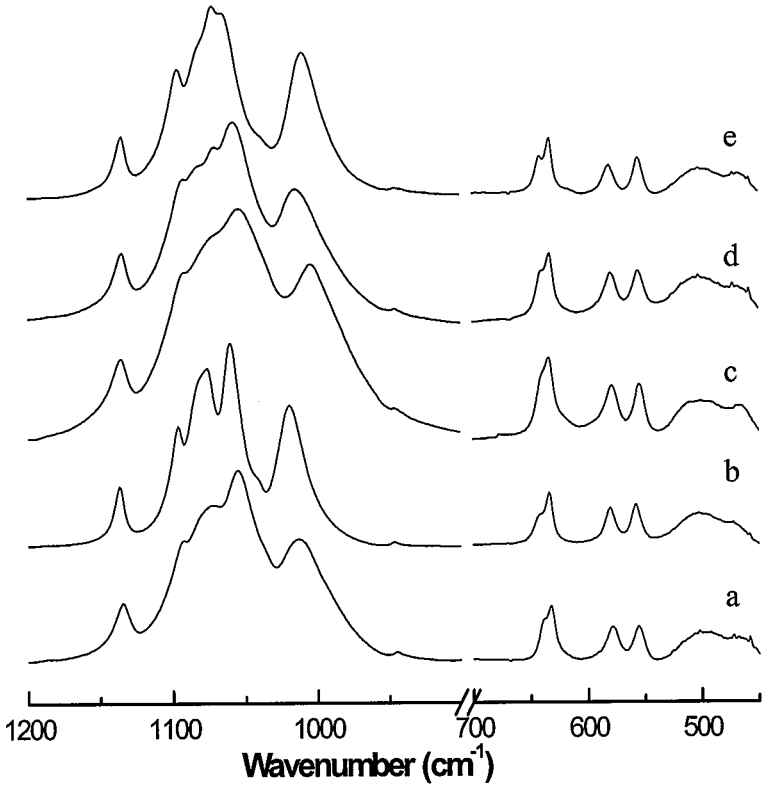

b)

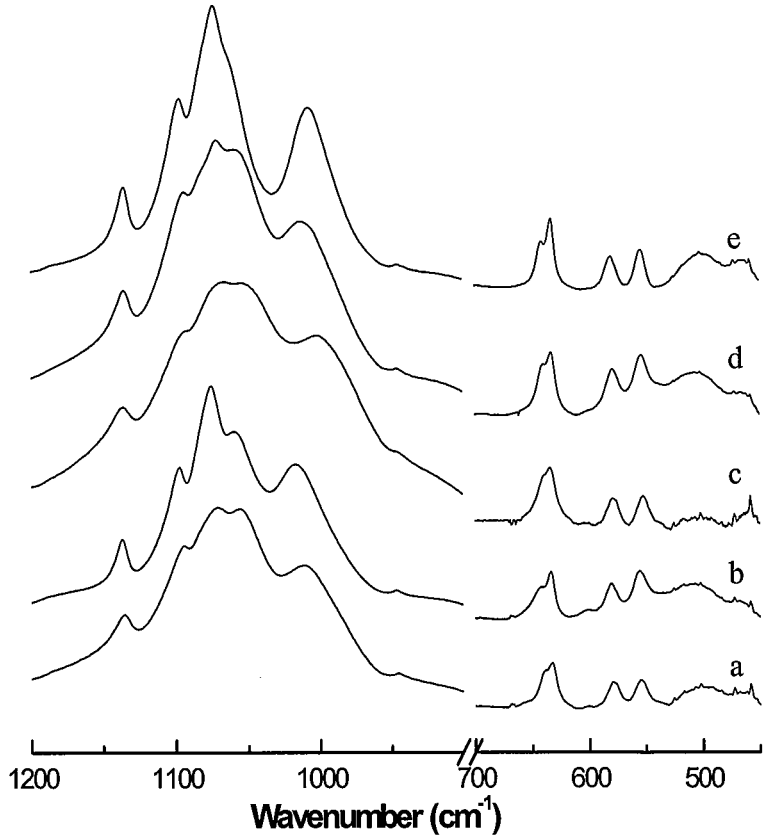

Chen and Richardson, Figure 5

a)

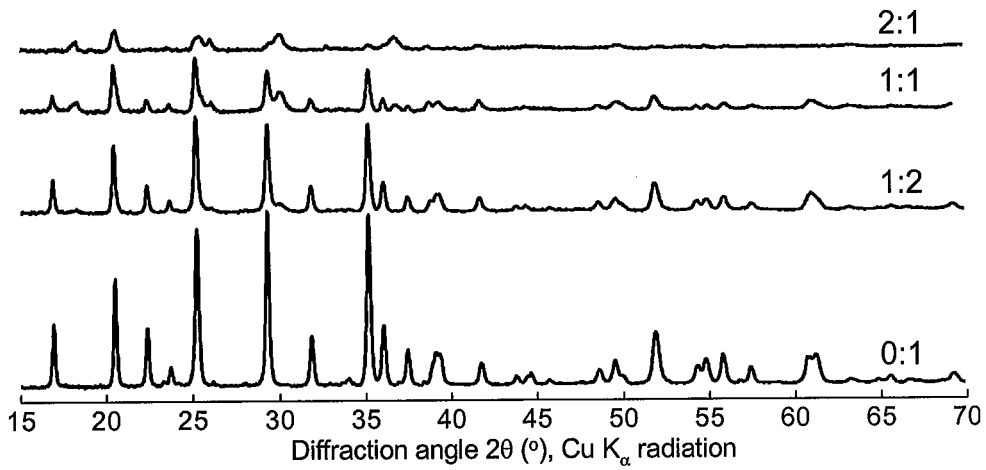

b)

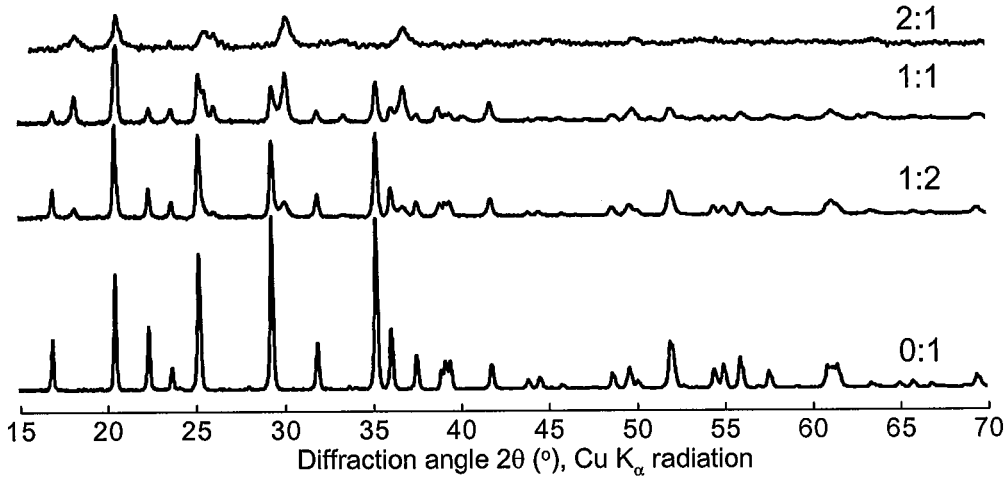

c)

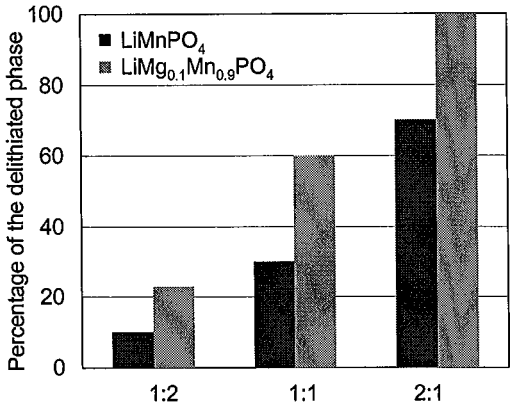

Chen and Richardson, Figure 6